PULMONARY NODULE DETECTION USING LOCAL CONTRAST THRESHOLDING WITH CIRCULAR WINDOW (CWLCT)

Dnyaneshwar Kanade* and Jagdish Helonde

Received: May 04, 2023; Revised: October 09, 2023; Accepted: January 12, 2024

Abstract

According to WHO, lung cancer is one of the major causes of cancer deaths worldwide. Lung nodule detection has substantially improved by using image processing techniques and Computer Aided Diagnosis (CAD) systems. A novel method is presented for processing Postero Anterior chest radiographs for extracting a candidate nodule based on their local properties using circular window-based local contrast thresholding (CWLCT). The algorithm is tested on different subtlety levels of chest radiographs and compared with square window-based Bernsen local contrast thresholding. For the first test 50 chest radiograph images with different subtlety levels are used. The experimental results of candidate nodule extraction using local contrast thresholding with a circular window show that for 90% of images true positive nodules are extracted accurately with minute error in the size and 4 false positive nodules/image. In the second test, the proposed method is compared with square window-based Bernsen local contrast thresholding and showed a reduction of 3.8 % in nodule size error. Utilizing CWLCT not only lowers the number of false positive nodules per picture but also assists in precisely segmenting nodules from chest radiograph images.

Keywords: **Active Shape Model; Bernsen; Chest Radiograph; Local Contrast Thresholding; Lung Cancer**

Introduction

Among the all-cancer deaths in the world, Lung cancer is one of the major causes. Radiography, computed tomography (CT), and magnetic resonance imaging (MRI) are the major imaging techniques used for the early detection of Lung cancer. Despite more accuracy and sensitivity of the CT and MRI techniques, radiography is still the most preferred technique for the early detection and diagnosis of lung cancer due to its noninvasively characteristics, radiation dose, and economy. Extracting lung parts from the chest radiograph and detecting candidate nodules from the segmented lungs are necessary steps before classifying them based on their features. Many researchers have proposed different techniques for detecting lung nodule-like parts in the chest radiograph. The local properties of the nodule may be affected by inaccurate segmentation of the nodule from the chest radiograph. The proposed work deals with the detection of nodule-like parts from the segmented

Department of Electrical & Electronics Engineering, School of Engineering and Technology, Sandip University, India. E-mail: dnyaneshwar.kanade@vit.edu; jbhelonde60@gmail.com

* *Corresponding author*

DOI: https://doi.org/10.55766/sujst-2024-01-e01140

lungs using CWLCT (Kanade and Helonde, 2023). The CWLCT is based on the Bernsen Local Contrast thresholding technique using a circular window instead of a square window. The diameter of the circular window is equal to the size of the square window. The lung masks are extracted using the Active Shape Model (ASM) (Cootes *et al*., 1994; Van Ginneken *et al*., 2002; Lee *et al*., 2009), which is the most robust segmentation technique. The most common diagnostic examination for cardiopulmonary abnormalities is a chest X-ray. However, subtle abnormalities can be obscured by bony structures like ribs and clavicles, leading to diagnostic errors. A deep learning (DL)-based (Rajaraman *et al*., 2021) bone suppression model that identifies and eliminates these occluding bony structures in frontal chest radiographs was proposed. A convolutional neural filter (CNF) (Matsubara *et al*., 2019) for bone suppression was proposed, which was based on a convolutional neural network that has excellent image processing performance and is frequently utilized in the medical field. The system resulted in bone suppression of 89.2% by using CNF with six convolutional layers. Using (Juhász *et al*., 2010; Horváth *et al*., 2013) dynamic programming, images are first segmented to remove rib and clavicle shadows. In different spaces, the segmented shadows are eliminated. A hybrid lesion detector based on gradient convergence, contrast, and intensity statistics processes the cleaned images. A Support Vector Machine eliminates false findings. About 80% of bone shadows can be removed. The proposed CWLCT-based method uses the Japanese Society of Radiological Technology (JSRT) (Juhász *et al*., 2010; Al Gindi *et al*., 2014) bone shadow eliminated dataset. At the state of the art, classical techniques based on several lung nodule segmentation methods have been presented. The use of a Gaussian filter for detecting nodules was implemented (Soleymanpour *et al*., 2011) with the assumption that nodules are circular. The smoothed images from the multi-scale Gaussian filter summed up, which resulted in the prominent appearance of the nodule. This work resulted in a huge number of false positive nodules for all 247 images with a sensitivity of 0.96. Extending previous work (Campadelli *et al*., 2006) for minimizing false positive nodules, the SVM classifier is used and reported the 0.71 a sensitivity for 1.5 false positive nodules/image. A method for enhancing (Shi *et al*., 2010) dot-like regions using directional Laplacian of Gaussian (LoG) was proposed. The main weakness of the method (Shi *et al*., 2010; Soleymanpour *et al*., 2011) is that it is based on assumptions regarding the equal subtlety level. Using (Patil and Udupi, 2010), global threshold value nodules were segmented from the chest radiographs, and true positive nodules were classified using geometrical and texture features. The forward stepwise selection method was (Wei *et al*., 2002) used to select the best feature set out of 210. The optimal feature set achieves a true positive detection rate of 80% and achieves an average of just 5.4 false positives per image. Otsu's thresholding (Mya *et al*., 2014) was used for detecting nodules from CT scan images. Since CT scan images are clearer than X-ray images, the same thresholding method does not produce effective results for X-rays. Statistical and geometrical features were calculated, and using the ANN classifier, the cancer stage was detected. A CAD system (Al Gindi *et al*., 2014) for lung nodule characterization and classification of nodules as benign or malignant using multiscale wavelet transform resulted in prominent results with a lot of computations. A method for suppressing (Chen and Suzuki, 2013) ribs and clavicles in the virtual dual-energy (VDE) image is implemented using the MTANN technique, which improves the visibility of the nodules obstructed by clavicles and ribs. The system does not include any nodule extraction technique. Three different methods (Savithri and Devi, 2016) for nodule extraction from chest radiographs were proposed. All three methods assume an equal subtlety levels of images. The features from the patch (the region of interest) were found using restricted Boltzmann, and a linear SVM classifier was used to classify the ROI as either nodule or non-nodule. By using Lindeberg's multiscale blob detector (Schilham *et al*., 2003) the detection of the candidate nodules in the chest radiograph is performed. It provided sensitivity greater than 50% for 2 false positives per image, and 70% for 10 false positives per image. The assumption of equal subtlety level for all images is the main drawback of the system. Thresholding techniques are widely used in image binarization (Mehmet and Bulent, 2004). Thresholding techniques (Singh *et al*., 2011; Nie *et al*., 2013) are broadly classified as clustering-based methods, histogram shape-based methods, entropy-based methods, object attribute-based methods, spatial methods, and local methods. These methods adjust the threshold value for each pixel based on the image's local features. A detailed comparative study of (Chaya Devi and Satya Savithri, 2018) different algorithms methods used for rib suppression from chest radiographs, lung segmentation algorithms, candidate nodule detection, estimating their features, and classifying them as nodule or non-nodule was established. A comparative study of different lung nodule segmentation techniques (Zheng and Lei, 2018) was proposed. The proposed system used active contour, differential operator and region growing techniques for nodule segmentation. Deep learning based (Liang *et al*., 2020) CAD system for detecting pulmonary nodules from chest radiographs was proposed. The proposed system used four algorithms: abnormal probability algorithm, nodule probability algorithm, heat map algorithm, and mass probability algorithm. This proposed system established a comparative study based on the performance of these algorithms. A total of 100 cases were used for analysis purposes, and among the four algorithms, the mass probability algorithm performed well, achieving a sensitivity of 76.6% and a specificity of 88.68%. A hybrid neural network method (Bharati *et al*., 2020) was proposed to overcome the limitations of CNN by combining it with a visual geometry group based neural network, spatial transformer network, and data augmentation. Region growing based nodule segmentation method (Soltani-Nabipour *et al*., 2020) was proposed. The region grown from the seed point was restricted by priori knowledge which resulted in the accurate segmentation of nodules. A novel decision tree-based computer vision model and hybrid deep learning (Horry *et al*., 2021) method was proposed. The deep learning module was trained with a large number of ground truth images from the JSRT dataset. Malignancy scattered datasets were applied to the shallow decision tree model, and the best-fitted model from multivariate predictive models was determined. The method archives specificity and sensitivity of 80.0% and 86.7%, respectively. The model also obtained a 92.9% positive predictive rate. Most of these research works assumed an equal subtlety level of all the images, and often, this assumption was violated in real-life situations. Despite of using these assumptions and by applying some prior essential knowledge to the nodule shape, other proposed methods obtained better results. Major features of the nodule may be lost by the loss of parts of the nodule area and may result in inaccurate classification of the true positive nodules. Precision is the most important parameter to minimize the number of false positive cases while segmenting the candidate nodules. The success of the further classification of true positive nodules from the candidate nodules based on statistical features depends on the number of false positive nodules as part of candidate nodules.

A. Locally adaptive thresholding

Threshold $T_n(x, y)$ is a value in locally adaptive thresholding and

$$b_n(x,y) = \begin{cases} 0 & if\ I(x,y) \leq T_n(x,y) \\ 1 & otherwise \end{cases} \quad (1)$$

where the binarized image is denoted by bn(x,y) and pixel (x,y) intensity of the image I is denoted by I(x,y). A threshold is determined for every pixel in the local adaptive technique, which is based on statistical parameters (Mehmet and Bulent, 2004). Background subtraction, mean value of pixel values, standard deviation, local image contrast, and water flow model are major different approaches of local adaptive technique. The major drawbacks of local adaptive thresholding techniques are that they depend on the region size and characteristics of each image. They are also time-consuming. A combination of global and local thresholding (Savithri and Devi, 2016) approaches are also proposed, as well as the usage of morphological operators. The local variance technique (Singh *et al*., 2011) is used by Niblack, Sauvola, and Pietaksinen, while the midrange value inside the local block is used by Bernsen.

B. Bernsen local contrast thresholding

The threshold is set at the midway value in the original Bernsen local contrast thresholding technique (J. Bernsen, 1986), which is the mean of the least Ilow(p, q) and maximum Ihigh(p, q) grey values in a local window of size w. The method uses a user-provided contrast threshold. If the contrast C(p, q) = Ihigh(p, q) - Ilow(p, q) is less than a particular threshold, the neighborhood is said to have only one class, foreground or background, depending on T(p, q). Bernsen local contrast thresholding employs a w × w square window.

$$T(p,q) = 0.5\{max_w[\,l(p+m,q+n)] + min_w[\,l(p+m,q+n)]\} \quad (2)$$

provided local contrast is

$$C(p,q) = I_{high}(p,q) - I_{low}(p,q) \geq 15 \quad (3)$$

The drawback of Bernsen local contrast thresholding-based image binarization is the square window of size w×w used for calculating local contrast. The suggested system’s primary goal is to promote the development of a novel method of binarization to extract the true positive nodule with a minimum % error in nodule dimensions as compared with the original one.

Materials and methods

The following assumptions are made before applying the proposed method for candidate nodule extraction from chest radiographs using local contrast thresholding with a circular-window. The dataset used for the proposed method is Japanese

Society of Radiological Technology (JSRT) (Junji *et al*., 2000) digital chest radiograph images without bone shadow (Horváth *et al*., 2013; Juhász *et al*., 2010). The dataset consists of 154 lung nodule chest radiographs and non-nodule 93 radiographs. Each chest radiograph of the JSRT dataset with lung nodule is having only one nodule. The images with subtlety level 5 (Nodule is obvious) to subtlety level 2 (Nodule is very subtle) are used for analysis. The images with subtlety level 1 (Extremely subtle) are not used in the proposed method since the extraction of a nodule is highly difficult because its contrast is low, size is small, or due to overlapping by normal structure. Similar post-processing is employed for both the proposed method and the previous method. The % error difference is computed for nodule area, third moment, and fourth moment.

A. Algorithm

As shown in Figure 1, the proposed method is divided into sub-processes, namely i) Pre-processing of the image, ii) Lung segmentation, iii) Image binarization, and iv) Post-processing of the image for maintaining the integrity of the specifications.

1). Pre-processing

In the pre-processing, the original chest radiograph images are enhanced for their contrast as shown in Figure 2a and down-sampled to 512×512 from their original size of 2048×2048 before using them for lung segmentation using ASM (Cootes et al., 1994).

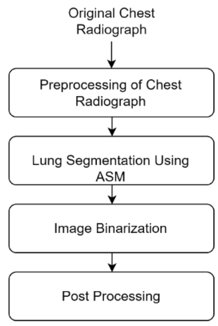

Figure 1. System flow chart

(a) (b) (c)

Figure 2. Lung Segmentation. (a) original chest radiograph, (b) ASM lung mask, and (c) lungs part of chest radiograph

2). Lung segmentation

Active Shape Model (ASM) (Cootes *et al*., 1994; Van Ginneken *et al*., 2002) is used for segmenting the lungs from the pre-processed original chest radiograph. ASM is one of the most robust algorithms used for image segmentation. The Active Shape Model is a contour model with parameters. Using principal component analysis (PCA) and the statistics of multiple sets of points derived from different contours of comparable images, the parameters are determined. The boundary of the object in ASM is determined by n points. The descriptor vector from these points is created as:

$$x = (x_1, y_1, x_2, y_2, \ldots, x_n, y_n)^T \quad (4)$$

Where x_i and y_i are x and y coordinates on *i-th* point on the contour. The s training vectors calculated for principal component analysis have a mean shape of

$$\bar{x} = \frac{1}{s}\sum_{i=1}^{s} x_i \quad (5)$$

The covariance matrix will be

$$S = \frac{1}{1-s}\sum_{i=1}^{s}(x_i - \bar{x})\,(x_i - \bar{x})^T \quad (6)$$

The first t largest Eigen values λ_i of the covariance matrix are chosen. Because only the most significant Eigenvalues are considered, the number of parameters is drastically reduced and falls below n. The matrix is filled with the corresponding eigenvectors. The model parameters are calculated as:

$$b = \Phi^T(x - \bar{x}) \quad (7)$$

from this the approximation of the shape is calculated as:

$$x \approx \bar{x} + \Phi b \quad (8)$$

An appropriate b vector is identified for a given contour such that all components of b are within the interval $\pm m\sqrt{\lambda i}$, with an appropriate constant m. The parametric description of an object's contour is searched starting with the mean shape. Two alternating steps are applied until convergence or a predetermined number of iterations are reached. In the first phase of the method, each contour point perpendicular to the contour is moved. The optimal position is found after multiple cycles of position testing on both sides of the contour. During the training model, picture resolution is employed to locate the optimal position of an intensity gradient profile at each contour node. Finally, Mahalanobis distance is used to identify the optimal new position for the contour point. Then, to fit a model to the new point set, all of the contour points are updated. According to Eq.8, the best b parameter is sought. The entire process is repeated several times as the spatial resolution of the image improves. For training the model we used 100 images from the JSRT dataset (Junji *et al*., 2000). Figure 2(a) shows the original chest radiograph. The segmented lung mask obtained using ASM is shown in Figure 2(b). The lungs are segmented by applying this mask to the original X-ray image, as shown in Figure 2(c).

3). Image Binarization

While calculating local contrast, the proposed method uses local contrast thresholding with a circular window (CWLCT), as shown in Figure 3(b), with diameter w for image binarization instead of a square window, as shown in Figure 3(a). For pixel P centered at i and j with a square window of size w×w takes 22% more neighbouring pixels into account than the circular window having diameter w. The circular window used in the proposed method for image binarization plays an important role while calculating the local contrast for the boundary pixels of the true positive nodule. The square window, as shown in Figure 4, takes more pixels of background into account while calculating local contrast and hence may detect the nodule pixel as belonging to the background, which may result in inaccurate estimation of the local properties of nodule-like parts in the chest radiograph. The original chest radiograph and the resulting image after image binarization are shown in Figure 5(a) and Figure 5(b), respectively.

4). Post processing

In post-processing, morphological operations are used for removing unwanted regions. Using prior knowledge of the true positive nodule, a substantial reduction in the false positive nodules is obtained. Based on the circularity index of the candidate nodules, the final candidate nodule segmented image is obtained. Figure 6(a) shows the original chest radiograph, while Figure 6(b) shows the image with candidate nodules in which the white nodule is true positive and the grey is false positive. Two tests are conducted for validating the performance of the proposed method. In test-150 images with subtlety levels 5 to 2 are selected and tested with CWLCT. In Test-2 images are binarized using local contrast thresholding using square window and CWLCT. The area of the true positive nodules is calculated and compared with the manually extracted true positive nodules from the chest radiograph for estimating the percentage error.

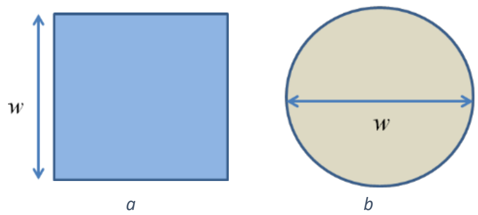

Figure 3. **Window (a) Square window and (b) Circular window**

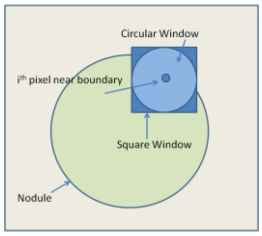

Figure 4. **Square window and circular window of local contrast thresholding cantered at boundary pixel i**

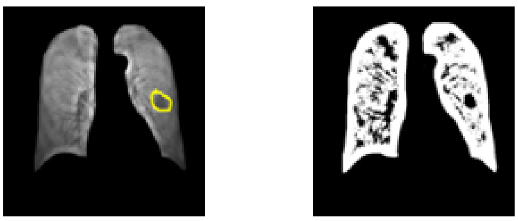

(a) (b)

Figure 5. **Local Contrast Thresholding. (a) original chest radiograph and (b) Binarization using local contrast thresholding**

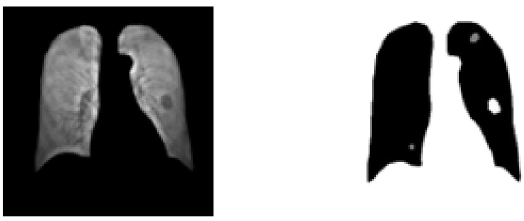

(a) (b)

Figure 6. **Local Contrast Thresholding. (a) original chest radiograph and (b) Binarization using local contrast thresholding**

Results and Discussion

As shown in the flow chart Figure 7, before applying CWLCT the chest radiographs are pre-processed for enhancing the nodule-like region's visibility. Then lungs are segmented using ASM. In this test, the proposed method was tested and it is found that 90 % of the true positive nodules extracted are part of candidate nodules. The true positive nodules are the nodules having been mentioned in the JSRT clinical information. The average rate of false positive nodules per image is 4.

Figures 8(a), 8(c), 8(e), and 8(g) show the original chest radiograph sample images with subtlety levels 5 to 2, respectively, while Figures 8(b), 8(d), 8(f), and 8(h) show nodule extraction results of the proposed method applied to sample images.

As shown in Figure 9, the sample images with subtlety levels 5 to 2 are undergone similar processes till the lung segmentation using ASM. Local contrast thresholding with a square window and CWLCT is used to binarize images. For the purpose of calculating the % error, the area of the true positive nodules is calculated and compared to the manually extracted genuine positive nodules from the chest radiograph. The proposed candidate nodule extraction method CWLCT results in a more accurate extraction of the true positive nodule when compared with the original local contrast thresholding with a square window. In many cases, the true positive nodule extracted using a square filter is either missed or smaller than the original size of the nodule or nodule extracted using CWLCT. Figure 10(a) and Figure 10(b) show the difference between nodule size when extracted using a square window and a circular window. We tested our candidate nodule extraction method on a rather substantial, relevant, and nontrivial 40 real-life cases, 10 from each group of JSRT dataset images with subtlety levels 5 to 2. Figures 8a, 8c, 8e, and 8g show the original chest radiograph sample images with subtlety levels 5 to 2, respectively, while Figures 8b, 8d, 8f, and 8h show nodule extraction results of the proposed method applied to sample images. Using the original size of the nodule given in the clinical information the % error is calculated for square window and circular window. To judge the obtained results, we compared the original square window-based Bernsen local contrast thresholding with the proposed method and came up with the following findings.

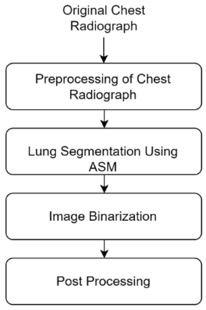

Figure 7. System flow chart for Test-1

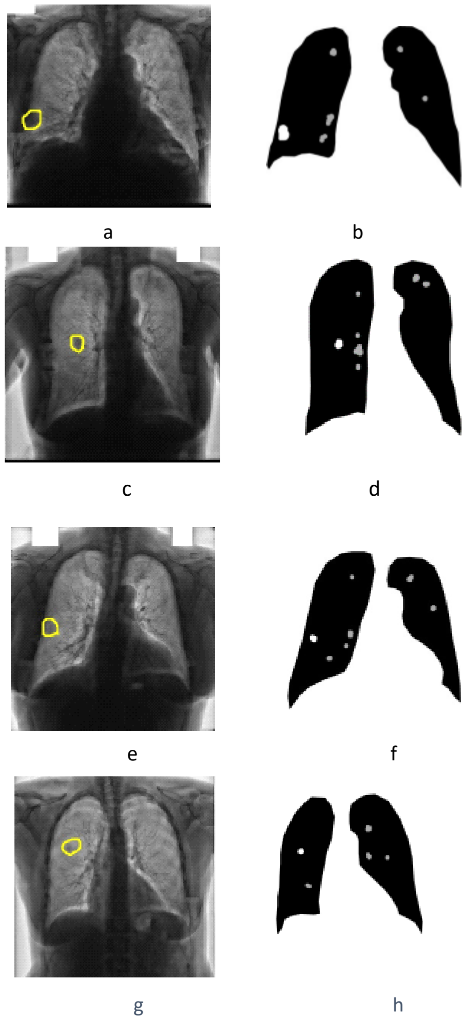

Figure 8. Some of the results obtained - Original Images with subtlety levels 5,4,3, and 2 sequentially (Left Column-(a), (c), (e), (g)), results of candidate nodule segmentation (White-True positive nodules) using local contrast thresholding and circular window (Right column-(b), (d), (f), (h))

1). Case 1: Images with subtlety level 5

From Figure 11, it can be observed that there is no significant difference between the proposed method and square window-based Bernsen local contrast thresholding except in one or two cases.

2.) Case 2: Images with subtlety level 4

As shown in Figure 12, with the square window-based Bernsen local contrast thresholding method, for 50% of the images the true positive nodule could not be extracted as compared to the proposed method. For the remaining cases, the square window-based Bernsen local contrast thresholding detected nodules with an average 24.4% error as compared to an 18.2% error for the proposed method.

3). Case 3: Images with subtlety level 3

As shown in Figure 13 with the square window-based Bernsen local contrast thresholding method, for 50% of the images, the true positive nodule could not be extracted as compared to the proposed method. For the remaining cases, the square window-based Bernsen local contrast thresholding detected nodules with an average 26.8% error as compared to a 26.2% error for the proposed method.

4). Case 4: Images with subtlety level 2

As shown in Figure 14, using the square window-based Bernsen local contrast thresholding method, for 40% of the images the true positive nodule could not be extracted as compared to the proposed method. For the remaining cases, the square window-based Bernsen local contrast thresholding detected nodules with an average 20.2% error as compared to an 18.2% error for the proposed method.

Average percentage error using square window for subtlety level 2 to 5 images can be calculated as

$$\%E_s = \frac{1}{4}\sum_{s=2}^{5} \overline{es}_s \tag{9}$$

Where es_s is average percentage error using square window for subtlety level s.

Average percentage error using circular window for subtlety level 2 to 5 images can be calculated as

$$\%E_c = \frac{1}{4}\sum_{s=2}^{5} \overline{ec}_s \tag{10}$$

Where ecs is average percentage error using circular window for subtlety level s.

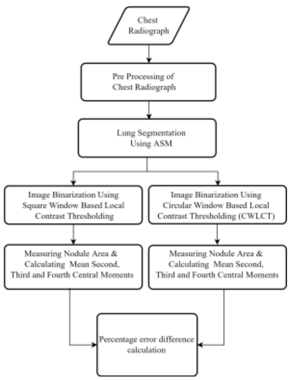

Figure 9. System flow chart for Test-1

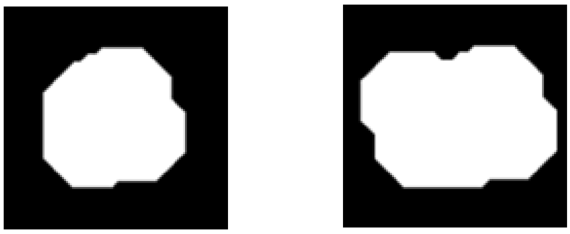

Figure 10. Nodule Segmentation (a) Using Square window and (b) Using circular window

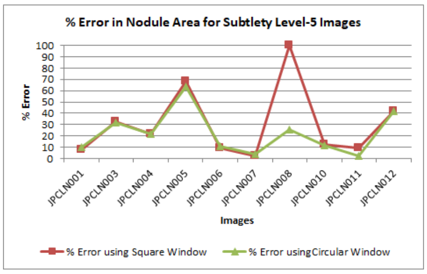

Figure 11. Percentage Error in nodule area using local contrast thresholding with square and circular window for subtlety level 5 images

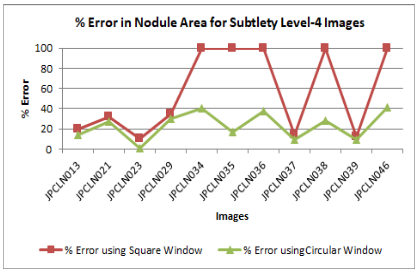

Figure 12. Percentage Error in nodule area using local contrast thresholding with square and circular window for subtlety level 4 images

Using Eq. 9 and Eq. 10, it is found that the average reduction in % error difference using the proposed CWLCT-based thresholding is improved by 3.8% as compared to the square window-based local contrast thresholding algorithm.

To analyze the results obtained as shown in Figures 11 to 14, we divided the data into two groups. Group 1 will represent the data for the maximum percentage error difference between a square window and a circular window and Group 2 will represent the data for the minimum percentage error difference between a square window and a circular window.

Table 1 shows sample images with nodule area % error difference between square window-based local contrast thresholding and proposed method to be maximum while Table 2 shows sample images with nodule area % error difference between square window based local contrast thresholding and proposed method to be minimum.

Table 3 shows % error difference for the third and fourth moment using square window-based local contrast thresholding and the proposed method to be maximum. Table 4 shows the % error difference for the third and fourth moments using square window-based local contrast thresholding and the proposed method to be minimum. From the Table 1 and Table 3, it can be observed that when nodule area % error difference between square window-based local contrast thresholding and the proposed method is maximum then % error difference for the third and fourth moment using square window-based local contrast thresholding and the proposed method is also maximum which is

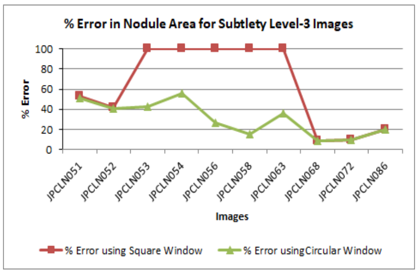

Figure 13. **Percentage Error in nodule area using local contrast thresholding with square and circular window for subtlety level 3 images**

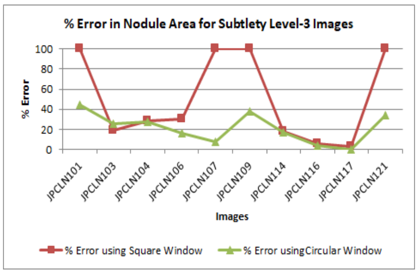

Figure 14. **Percentage Error in nodule area using local contrast thresholding with square and circular window for subtlety level 2 images**

Table 1. **Sample results of extracted nodule area for maximum % error difference between square and circular window (100% error means nodule not detected)**

JSRT X-Ray Image	% Error in Nodule Area	
	Using Square window	Using Circular
JPCLN008	100	26
JPCLN011	9	2
JPCLN023	10	0
JPCLN035	100	17
JPCLN038	100	28
JPCLN053	100	42
JPCLN054	100	56
JPCLN056	100	27
JPCLN107	100	8
JPCLN109	100	38

Table 2. **Sample results of extracted nodule area for minimum % error difference between square and circular window**

JSRT X-Ray Image	% Error in Nodule Area	
	Using Square window	Using Circular
JPCLN003	32	32
JPCLN005	69	64
JPCLN006	9	10
JPCLN012	42	42
JPCLN013	20	14
JPCLN021	32	28
JPCLN051	53	51
JPCLN052	42	41
JPCLN104	29	27
JPCLN114	18	17

shown in Figure 15 and 16. From Tables 2 and Table 4, it can be observed that when the nodule area % error difference between square window-based local contrast thresholding and the proposed method is minimum, then the % error difference for a third and fourth moment using square window-based local contrast thresholding and the proposed method is also minimum as shown in Figure 17 and Figure 18. When the nodule area difference between the original nodule and the nodule extracted using either square window-based local contrast thresholding or the proposed method is positive then the intensities of nodule pixels tend to produce a positively skewed distribution while the nodule area difference between the original nodule and the nodule extracted using either square window-based local contrast thresholding or proposed method is negative then the intensities of nodule pixels tend to produce negatively skewed distribution. Figure 15 and Figure 16 show the % error difference for the third moment and fourth moment of the extracted nodule using square window- based local contrast thresholding and CWLCT of Group-1 images.

Figure 17 and Figure 18 show the % error difference for the third moment and fourth moment of the extracted nodule using square window-based local contrast thresholding and CWLCT of Group-2 images.

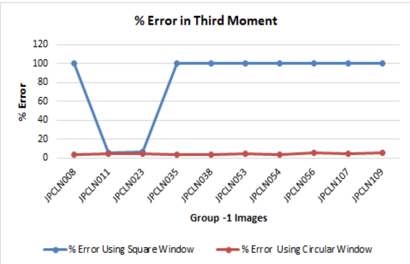

Figure 15. **Percentage Error in third moment using square and circular window for group 1 images**

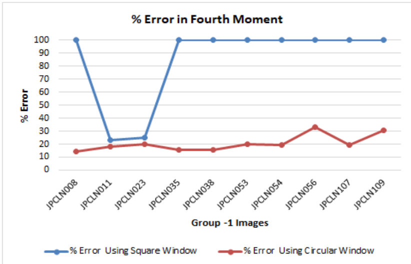

Figure 16. **Percentage Error in fourth moment using square and circular window for group 1 images**

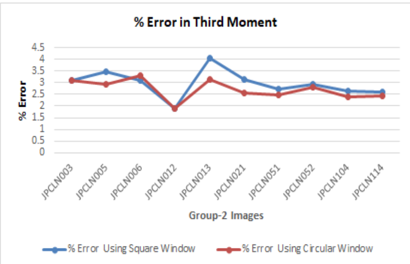

Figure 17. **Percentage Error in third moment using square and circular window for group 2 images**

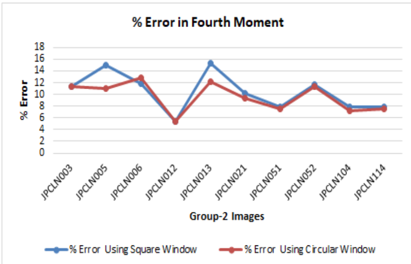

Figure 18. **Percentage Error in third moment using square and circular window for group 2 images**

Table 3. **Sample results of the second, third, and fourth central moment for maximum % error difference between the square and circular window. (100% error means nodule not detected)**

JSRT X-Ray Images	% Error Using Square Window		% Error Using Circular Window	
	Kurtosis	Skewness	Kurtosis	Skewness
JPCLN008	100	100	14.5966	3.5607
JPCLN011	23.1311	4.9341	18.2209	4.0161
JPCLN023	25.1291	6.3432	20.2314	4.2136
JPCLN035	100	100	15.7537	3.6546
JPCLN038	100	100	15.6721	3.6214
JPCLN053	100	100	19.9611	4.1583
JPCLN054	100	100	19.0394	3.9319
JPCLN056	100	100	33.4281	5.4326
JPCLN107	100	100	19.2131	4.1919
JPCLN109	100	100	30.9276	5.1732

Table 4. Sample results of second, third and fourth central moment for minimum % error difference between square and circular window

JSRT X-Ray Images	% Error Using Square Window		% Error Using Circular Window	
	Kurtosis	Skewness	Kurtosis	Skewness
JPCLN003	11.3218	3.0851	11.3218	3.0851
JPCLN005	14.9213	3.4619	10.9213	2.9109
JPCLN006	11.8181	3.1134	12.7594	3.2966
JPCLN012	5.3372	1.9047	5.3372	1.9047
JPCLN013	15.3187	4.0372	12.2207	3.1319
JPCLN021	10.1912	3.1211	9.3764	2.5761
JPCLN051	7.9416	2.7132	7.5125	2.4681
JPCLN052	11.6811	2.9159	11.3902	2.8157
JPCLN104	7.9132	2.6332	7.2401	2.3815
JPCLN114	7.9412	2.6041	7.4605	2.4145

Conclusion

With the aim of improving the accuracy of nodule detection proposed work of local contrast thresholding using CWLCT fulfils the aim. The experimental setup 1 (Test-1) with subtlety level 5 to 2 chest radiograph images detects the true positive nodules with 90% accuracy, which substantially reduces the number of false positive nodules per image. In experimental setup 2 (Test-2), the existing and CWLCT binarization methods were employed, and the area of nodules was extracted using square window-based local contrast thresholding and the proposed CWLCT method. It is observed that extraction performance is improved by 3.8% using the proposed CWLCT method as compared to local contrast thresholding using a square window. The third and fourth moments for the Group-1 and Group-2 images obtain the same results as those obtained for the nodule area. In summary, the use of CWLCT not only reduces the false positive nodules per image but also helps in segmenting nodules accurately from the chest radiograph images.

References

Al Gindi, A.M., Rashed, E.A., and Mostafa, M.-S. M. (2014). Development and Evaluation of a Computer-Aided Diagnostic Algorithm for Lung Nodule Characterization and Classification in Chest Radiographs using Multiscale Wavelet Transform. Journal of American Science, 10(2):1,545-1,003. http://www.jofamericanscience.orghttp://www.jofamericanscience.org.14

Bernsen, J. (1986). Dynamic thresholding of gray-level images. Proceedings International Conference on Pattern Recognition. pp. 1,251-1,255.

Bharati, S., Podder, P., and Mondal, M.R.H. (2020). Hybrid deep learning for detecting lung diseases from X-ray images. Informatics in Medicine Unlocked, 20:100391. https://doi.org/10.1016/j.imu.2020.100391

Campadelli, P., Casiraghi, E., and Artioli, D. (2006). A fully automated method for lung nodule detection from postero-anterior chest radiographs. IEEE Transactions on Medical Imaging, 25(12):1,588-1,603. https://doi.org/10.1109/TMI.2006.884198

Chaya Devi, S.K. and Satya Savithri, T. (2018). Review: On segmentation of nodules from posterior and anterior chest radiographs. International Journal of Biomedical Imaging, Vol. 2018. https://doi.org/10.1155/2018/9752638

Chen, S. and Suzuki, K. (2013). Computerized detection of lung nodules by means of “virtual dual-energy” radiography. IEEE Transactions on Biomedical Engineering, 60(2):369-378. https://doi.org/10.1109/TBME.2012.2226583

Cootes, T.F., Hill, A., Taylor, C., and Hastam, J. (1994). Use of active shape models for locating structures in medical images. Image and Vision Computing, 12(6):355-365. https://doi.org/10.1016/0262-8856(94)90060-4

Horry, M., Chakraborty, S., Pradhan, B., Paul, M., Gomes, D., and Ul-Haq, A. (2021). Deep Mining Generation of Lung Cancer Malignancy Models from Chest X-ray Images. Sensors (Basel), 21(19):6,655. https://doi.org/10.3390/s21196655

Horváth, Á., Orbán, G., Horváth, Á., and Horváth, G. (2013). An X-ray CAD system with ribcage suppression for improved detection of lung lesions. Periodica Polytechnica Electrical Engineering and Computer Science, 57(1):19-33. https://doi.org/10.3311/PPee.2079

Juhász, S., Horváth, Á., Nikházy, L., and Horváth, G. (2010). Segmentation of Anatomical Structures on Chest Radiographs. Medicon 2010, IFMBE Proceedings 29:359-362. www.springerlink.com. https://doi.org/10.1007/978-3-642-13039-7_90

Junji, S., Shigehiko, K., Junpei, I., Tsuneo, M., Takeshi, K., Ken-ichi, K., Mitate, M., Hiroshi, F., Yoshie, K., and Kunio, D. (2000). A Development of a Digital Image Database for Chest Radiographs With and Without a Lung Nodule: Receiver Operating Characteristic Analysis of Radiologists’ Detection of Pulmonary Nodules. American Journal of Roentgenology, 174(1):71-74. https://doi.org/10.2214/ajr.174.1.1740071.

Kanade D. and Helonde J. (2023). Suppressing Chest Radiograph Ribs for Improving Lung Nodule Visibility by using Circular Window Adaptive Median Outlier (CWAMO). International Journal of Advanced Computer Science and Applications (IJACSA), 14(3):2,023. http://dx.doi.org/10.14569/IJACSA.2023.0140359

Lee, J.-S., Wu, H.-H., and Yuan, M.-Z. (2009). Lung Segmentation for Chest Radiograph by Using Adaptive Active Shape Models. 2009 Fifth International Conference on Information Assurance and Security, Xi’an, China, pp. 383-386. https://doi.org/10.1109/IAS.2009.353

Liang, C.H., Liu, Y.C., Wu, M.T., Garcia-Castro, F., Alberich-Bayarri, A., and Wu, F.Z. (2020). Identifying pulmonary nodules or masses on chest radiography using deep learning: external validation and strategies to improve clinical practice. Clinical Radiology, 75(1):38-45. https://doi.org/10.1016/j.crad.2019.08.005

Matsubara, N., Teramoto, A., Saito, K., and Fujita, H. (2019). Bone suppression for chest X-ray image using a convolutional neural filter. Australasian Physical and Engineering Sciences in Medicine, 43:97-108. https://doi.org/10.1007/s13246-019-00822-w

Mehmet, S. and Bulent, S. (2004). Survey over image thresholding techniques and quantitative performance evaluation. Journal of Electronic Imaging, 13(1):146-165. https://doi.org/10.1117/1.1631316

Mya, K., Tun, M., and Soe Khaing, A. (2014). Feature Extraction and Classification of Lung Cancer Nodule using Image Processing Techniques. International Journal of Engineering Research and Technology, 3(3).

Nie, F., Wang, Y., Pan, M., Peng, G., and Zhang, P. (2013). Two-dimensional extension of variance-based thresholding for image segmentation. Multidimensional Systems and Signal Processing, 24(3):485-501. https://doi.org/10.1007/s11045-012-0174-7

Patil, S.A. and Udupi, V.R. (2010). Chest X-ray features extraction for lung cancer classification. Journal of Scientific & Industrial Research, 69:271-277.

Rajaraman, S., Zamzmi, G., Folio, L., Alderson, P., & Antani, S. (2021). Chest X-Ray Bone Suppression for Improving Classification of Tuberculosis-Consistent Findings. Diagnostics (Basel), 11(5):840. https://doi.org/10.3390/diagnostics11050840

Savithri, T.S. and Devi, S.K.C. (2016). Nodule detection from posterior and anterior chest radiographs with different methods. 2016 Future Technologies Conference (FTC), San Francisco, pp. 504-515. https://doi.org/10.1109/FTC.2016.7821655

Schilham, A.M.R., van Ginneken, B., and Loog, M. (2003). Multi-scale Nodule Detection in Chest Radiographs. In: Ellis, R.E., Peters, T.M. (eds) Medical Image Computing and Computer-Assisted Intervention - MICCAI 2003. MICCAI 2003. Lecture Notes in Computer Science, vol 2878. Springer, Berlin, Heidelberg. https://doi.org/10.1007/978-3-540-39899-8_74

Shi, Z., Bai, J., Suzuki, K., He, L., Yao, Q., and Nakamura, T. (2010). A Method for Enhancing Dot-like Regions in Chest X-rays Based on Directional Scale LoG Filter. Journal of Information & Computational Science, 7(8):1,689-1,696. http://www.joics.com

Singh, T.R., Roy, S., Singh, O.I., Sinam, T., and Singh, K.M. (2011). A New Local Adaptive Thresholding Technique in Binarization. International Journal of Computer Science, 8(6). www.IJCSI.org.

Soleymanpour, E., Pourreza, H. R., Ansaripour, E., and Yazdi, M. S. (2011). Fully Automatic Lung Segmentation and Rib Suppression Methods to Improve Nodule Detection in Chest Radiographs. Journal of Medical Signals and Sensor, 1:191-199.

Soltani-Nabipour, J., Khorshidi, A., and Noorian, B. (2020). Lung tumor segmentation using improved region growing algorithm. Nuclear Engineering and Technology, 52(10):2,313-2,319. https://doi.org/10.1016/j.net.2020.03.011

Van Ginneken, B., Frangi, A.F., Staal, J.J., Ter Haar Romeny, B.M., and Viergever, M.A. (2002). Active shape model segmentation with optimal features. IEEE Transactions on Medical Imaging, 21(8):924-933. https://doi.org/10.1109/TMI.2002.803121

Wei, J., Hagihara, Y., Shimizu, A., and Kobatake, H. (2002). Optimal image feature set for detecting lung nodules on chest X-ray images. In: Lemke, H.U., Inamura, K., Doi, K., Vannier, M.W., Farman, A.G., Reiber, J.H.C. (eds) CARS 2002 Computer Assisted Radiology and Surgery. Springer, Berlin, Heidelberg. https://doi.org/10.1007/978-3-642-56168-9_118

Zheng, L. and Lei, Y. (2018). A Review of Image Segmentation Methods for Lung Nodule Detection Based on Computed Tomography Images. MATEC Web of Conferences, 232. https://doi.org/10.1051/matecconf/201823202001